ICCC 2004

2004 International Conference on Computational Cybernetics

Proceedings

Vienna, Austria - August 30 - September 1, 2004

Hungarian Fuzzy Association

Budapest Tech, Hungary

Vienna University of Technology, Austria

IEEE SMC Chapter, Hungary

IEEE NN Chapter, Hungary

IEEE Joint Chapter of IES and RAS, Hungary

IEEE R8

IEEE Systems, Man, and Cybernetics Society

EUROFUSE

Japan Society for Fuzzy Theory and Intelligent Informatics

John von Neumann Computer Society, Budapest, Hungary

IEEE

Fractional-Order Position/Force Robot Control

N. M. Fonseca Ferreira
Dept. of Electrical Engineering
Institute of Engineering of Coimbra
Rua Pedro Nunes - Quinta da Nora
3031-601 Coimbra Codex, Portugal
email: nunomig@isec.pt

J. A. Tenreiro Machado
Dept. of Electrical Engineering
Institute of Engineering of Porto
Rua Dr Ant. Bernardino de Almeida
4200-072 Porto Codex, Portugal
email: jtm@dee.isep.ipp.pt

J. Boaventura Cunha
Dept. of Electrical Engineering
University of Trás dos Montes e
Alto Douro, Ap 1013
5000-911 Vila Real, Portugal
email: jboavent@utad.pt

Abstract

This paper presents the implementation of fractional-order algorithms both for hybrid and cascade position/force control of robotic manipulators. The system performance and robustness is analyzed in the time and frequency domains. The effects joint backlash and flexibility are also investigated.

1. Introduction

In the early eighties Raibert and Craig [1] introduced the concept of force control based on the hybrid algorithm. Since then, several researchers [2-3] developed these ideas and proposed new algorithms such as the impedance controller. Problems with position/force control are further investigated in [3], while more recent studies of this algorithm can be found in [4-7].

There are two basic methods for force control, namely the hybrid position/force and the impedance schemes. The first algorithm [1] separates the task into two orthogonal subspaces corresponding to the force and the position subspaces. Once established the subspace decomposition two independent controllers are designed. Alternatively, with the second algorithm [2], by a proper choice of the arm impedance, the interaction forces can be accommodated to obtain an adequate response.

This paper studies the position/force control of robot manipulators, required in processes that involve contact between the gripper and the environment, using fractional-order (*FO*) algorithms. The application of the theory of fractional calculus is still in a research stage, but the recent progress in this area reveals promising aspects for future developments [6, 9].

In this line of thought the article is organized as follows. Sections two and three introduce the hybrid (HC) and the cascade (CC) controllers and the fundamentals of the *FO* algorithms, respectively. Section four analyses several experiments for the performance evaluation of two strategies, namely the *FO* and the *PID* controllers, for robots having several joint dynamical phenomena. Finally, section five outlines the main conclusions.

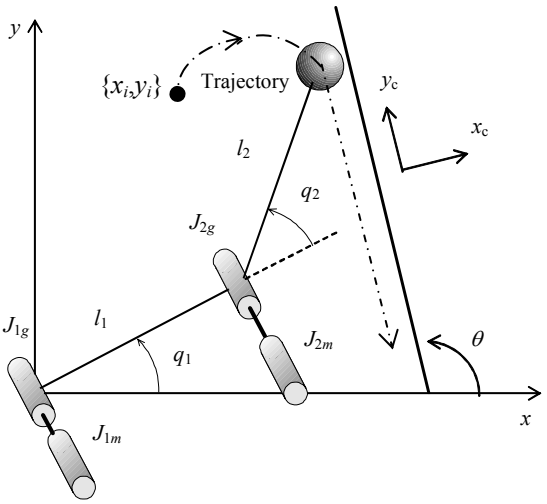

Figure 1 - The 2*R* robot and the constraint surface.

2. The Hybrid Controller

The dynamical equation of a *n* dof robot is:

$$\boldsymbol{\tau} = \mathbf{H}(\mathbf{q})\ddot{\mathbf{q}} + \mathbf{C}(\mathbf{q},\dot{\mathbf{q}}) + \mathbf{G}(\mathbf{q}) - \mathbf{J}^{\mathbf{T}}(\mathbf{q})\mathbf{F} \qquad (1)$$

where $\boldsymbol{\tau}$ is the $n \times 1$ vector of actuator torques, $\mathbf{q}$ is the $n \times 1$ vector of joint coordinates, $\mathbf{H(q)}$ is the $n \times n$ inertia matrix, $\mathbf{C(q,\dot{q})}$ is the $n \times 1$ vector of centrifugal/Coriolis terms and $\mathbf{G(q)}$ is the $n \times 1$ vector of gravitational effects. The $n \times m$ matrix $\mathbf{J^T(q)}$ is the transpose of the Jacobian of the robot and $\mathbf{F}$ is the $m \times 1$ vector of the force that the (m-dimensional) environment exerts in the gripper.

In this study we adopt the 2*R* robot (Fig. 1) with dynamics:

$$\mathbf{H}(\mathbf{q}) = \begin{bmatrix} (m_1+m_2)r_1^2 + m_2 r_2^2 + 2m_2 r_1 r_2 C_2 + J_{1m} + J_{1g} & m_2 r_2^2 + m_2 r_1 r_2 C_2 \\ m_2 r_2^2 + m_2 r_1 r_2 C_2 & m_2 r_2^2 + J_{2m} + J_{2g} \end{bmatrix} \qquad (2a)$$

$$\mathbf{C}(\mathbf{q},\dot{\mathbf{q}}) = \begin{bmatrix} -m_2 r_1 r_2 S_2 \dot{q}_2^{\,2} - 2m_2 r_1 r_2 S_2 \dot{q}_1 \dot{q}_2 \\ m_2 r_1 r_2 S_2 \dot{q}_1^{\,2} \end{bmatrix} \quad (2b)$$

$$\mathbf{G}(\mathbf{q}) = \begin{bmatrix} g(m_1 r_1 C_1 + m_2 r_1 C_1 + m_2 r_2 C_{12}) \\ g m_2 r_2 C_{12} \end{bmatrix} \quad (2c)$$

$$\mathbf{J}^{\mathbf{T}}(\mathbf{q}) = \begin{bmatrix} -r_1 S_1 - r_2 S_{12} & r_1 C_{11} + r_2 C_{12} \\ -r_2 S_{12} & r_2 C_{12} \end{bmatrix} \quad (2d)$$

where $C_{ij} = \cos(q_i + q_j)$ and $S_{ij} = \sin(q_i + q_j)$.

The numerical values adopted for the robot are $m_1 = 0.5$ kg, $m_2 = 6.25$ kg, $r_1 = 1.0$ m, $r_2 = 0.8$ m, $J_{1m} = J_{2m} = 1.0$ kgm^2 and $J_{1g} = J_{2g} = 4.0$ kgm^2 [6].

The constraint plane is determined by the angle θ (Fig. 1) and the contact displacement x_c of the robot gripper with the constraint surface is modeled through a linear system with a mass M, a damping B and a stiffness K with dynamics:

$$F_c = M\ddot{x}_c + B\dot{x}_c + Kx_c \quad (3)$$

The first control architecture consists on the *HC* algorithm (Fig. 2). The diagonal $n \times n$ selection matrix **S** has elements equal to one (zero) in the position (force) controlled directions and **I** is the $n \times n$ identity matrix. In this paper the y_c (x_c) cartesian coordinate is position (force) controlled, yielding:

$$\mathbf{S} = \begin{bmatrix} 0 & 0 \\ 0 & 1 \end{bmatrix}, \ \mathbf{J}_c(\mathbf{q}) = \begin{bmatrix} -r_1 C_{\theta 11} - r_2 C_{\theta 12} & -r_2 C_{\theta 12} \\ r_1 S_{\theta 11} + r_2 S_{\theta 12} & r_2 S_{\theta 12} \end{bmatrix} \quad (4)$$

where $C_{\theta ij} = \cos(\theta - q_i - q_j)$ and $S_{\theta ij} = \sin(\theta - q_i - q_j)$.

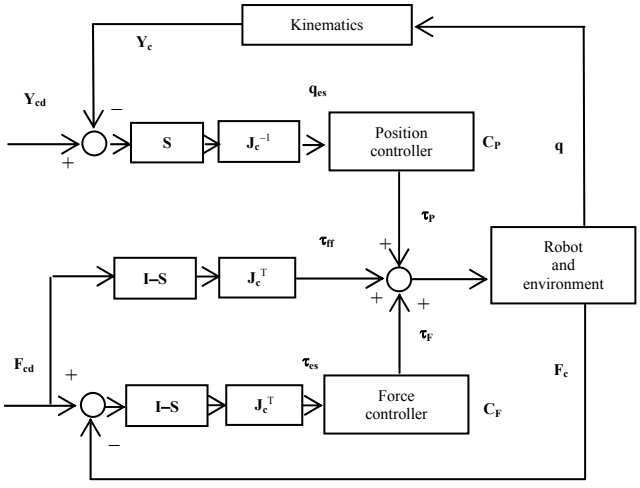

Figure 2 – The position/force hybrid controller.

The *CC* architecture (Fig. 3) is inspired on the impedance and compliance schemes. Therefore, we establish a cascade of force and position algorithms as internal an external feedback loops, respectively, where $\boldsymbol{x}_\mathbf{d}$ and $\boldsymbol{F}_\mathbf{d}$ are the payload desired position coordinates and contact forces.

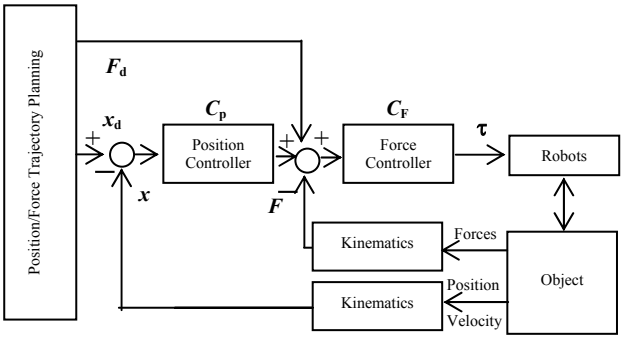

Figure 3 – The position/force cascade controller.

3. Fractional Order Algorithms

In this section we present the *FO* algorithms inserted at the position and force control loops.

The mathematical definition of a derivative of fractional order α has been the subject of several different approaches. For example, we can mention the Laplace and the Grünwald-Letnikov definitions:

$$D^{\alpha}[x(t)] = L^{-1}\{s^{\alpha} X(s)\} \quad (5a)$$

$$D^{\alpha}[x(t)] = \lim_{h \to 0}\left[\frac{1}{h^{\alpha}} \sum_{k=1}^{\infty} \frac{(-1)^k \Gamma(\alpha+1)}{\Gamma(k+1)\Gamma(\alpha-k+1)} x(t-kh)\right] \quad (5b)$$

where Γ is the gamma function and h is the time increment. In our case, for implementing *FO* algorithms of the type $C(s) = K_0 + K\, s^{\alpha}$, $-1 < \alpha < 1$, we adopt a 4$^{\text{th}}$-order discrete-time Pade approximation ($a_i, b_i, c_i, d_i \in \Re$, $k = 4$):

$$C_P(z) \approx K_P \frac{a_0 z^k + a_1 z^{k-1} + .. + a_k}{b_0 z^k + b_1 z^{k-1} + ... + b_k} \quad (6a)$$

$$C_F(z) \approx K_F \frac{c_0 z^k + c_1 z^{k-1} + .. + c_k}{d_0 z^k + d_1 z^{k-1} + ... + d_k} \quad (6b)$$

where K_P and K_F are the position and force loop gains, respectively.

4. Controller Performances

This section analyzes the system performance both for ideal transmissions and robots with dynamic phenomena at the joints, namely backlash and flexibility. Furthermore, we compare the response classical *PID* and *FO* algorithms for the integer–order case we adopt a *PD*: $C_P(s) = K_p + K_d\, s$ and a *PI*: $C_F(s) = K_p + K_i\, s^{-1}$ controllers, in the position and force loops [1-3].

Both algorithms were tuned by trial and error having in mind getting a good performance in the two cases. The resulting parameters for the position/force *HC* were *FO*: $\{K_P, K_D, \alpha_P\} \equiv \{1.12\times10^3, 1.5\times10^{-3}, 1/2\}$, $\{K_F, K_I, \alpha_F\} \equiv \{5$ $6.23, 1.83\times10^{-3}, -1/5\}$ and *PD/PI*: $\{K_p, K_d\} \equiv \{10^4, 10^3\}$, $\{K_p, K_i\} \equiv \{10^3, 10^2\}$ for the position and force loops, respectively. The parameters for the *CC* are *FO*: $\{K_P, K_D, \alpha_P\} \equiv \{0.1259, 0.15\times10^{-3}, 1/2\}$, $\{K_F, K_I, \alpha_F\} \equiv \{10.59, 1.83\times10^{-3}, -1/5\}$ and *PD/PI*:

$\{K_p,K_d\}\equiv\{10^4,10^3\}$, $\{K_p,K_i\}\equiv\{10^2,10\}$ for the position and force loops, respectively. Moreover, it is adopted a loop trajectory starting at the operating point $\{x,y\}\equiv\{1,1\}$ in the open space, and having contact after one second with a constraint surface with parameters $\{\theta,M,B,K\}\equiv\{\pi/4,1,10,10^3\}$ and a controller sampling frequency f_c = 1 kHz.

In order to study the system dynamics, during the contact we apply, separately, rectangular pulses, at the position and force references, that is, we perturb the reference with $\{\delta y_{cd},\delta F_{cd}\} = \{10^{-1},0\}$.

A. Time response

Figures 4 and 5 depict the time response for the position/force hybrid controller and the figures 6 and 7 for the cascade controller both under the action of the *FO* or *PD/PI* algorithms. These figures reveal that the *FO* algorithm is more stable than the *PD/PI*.

We analyze the response of a 2*R* robot with dynamic backlash at the joints [8, 10]. For the *i*th joint gear, with clearance h_i, the backlash reveals impact phenomena between the inertias, which are modeled according with the Newton law yielding:

$$\dot{q}_i' = \frac{\dot{q}_i\left(J_{ii}-\varepsilon J_{im}\right)+\dot{q}_{im}J_{im}\left(1+\varepsilon\right)}{J_{ii}+J_{im}} \tag{7a}$$

$$\dot{q}_{im}' = \frac{\dot{q}_i J_i\left(1+\varepsilon\right)+\dot{q}_{im}\left(J_{im}-\varepsilon J_{ii}\right)}{J_{ii}+J_{im}} \tag{7b}$$

where $0 \le \varepsilon \le 1$ is a constant that defines the type of impact ($\varepsilon = 0$ inelastic impact, $\varepsilon = 1$ elastic impact) and $\dot{q}_i'$ and $\dot{q}_{im}'$ are the inertias velocities of the joint and motor after the collision, respectively. The parameter J_{ii} (J_{im}) stands for the link (motor) inertias of joint *i*. The numerical values adopted are h_i = 1.8 10^{-4} rad and ε_i = 0.8 (i = 1, 2).

We consider also 2*R* robot with compliant joints. For this case the dynamics corresponds to model (1) augmented by the equations:

$$\boldsymbol{\tau} = \mathbf{J_m}\ddot{\mathbf{q}}_\mathbf{m} + \mathbf{B_m}\dot{\mathbf{q}}_\mathbf{m} + \mathbf{K_m}\left(\mathbf{q_m}-\mathbf{q}\right) \tag{8a}$$

$$\mathbf{K_m}\left(\mathbf{q_m}-\mathbf{q}\right) = \mathbf{J}(\mathbf{q})\ddot{\mathbf{q}} + \mathbf{C}(\mathbf{q},\dot{\mathbf{q}}) + \mathbf{G}(\mathbf{q}) \tag{8b}$$

where $\mathbf{J_m}$, $\mathbf{B_m}$ and $\mathbf{K_m}$ are the $n \times n$ diagonal matrices of the motor and transmission inertias, damping and stiffness, respectively. In the simulations we adopt K_{mi} = 2 10^6 Nm rad^{-1} and B_{mi} = 10^4 Nms rad^{-1} (i = 1,2).

Figure 4 and 6 reveals that the *FO* algorithm is superior to the *PD/PI* in the cases with dynamical phenomena at the joints [8-9].

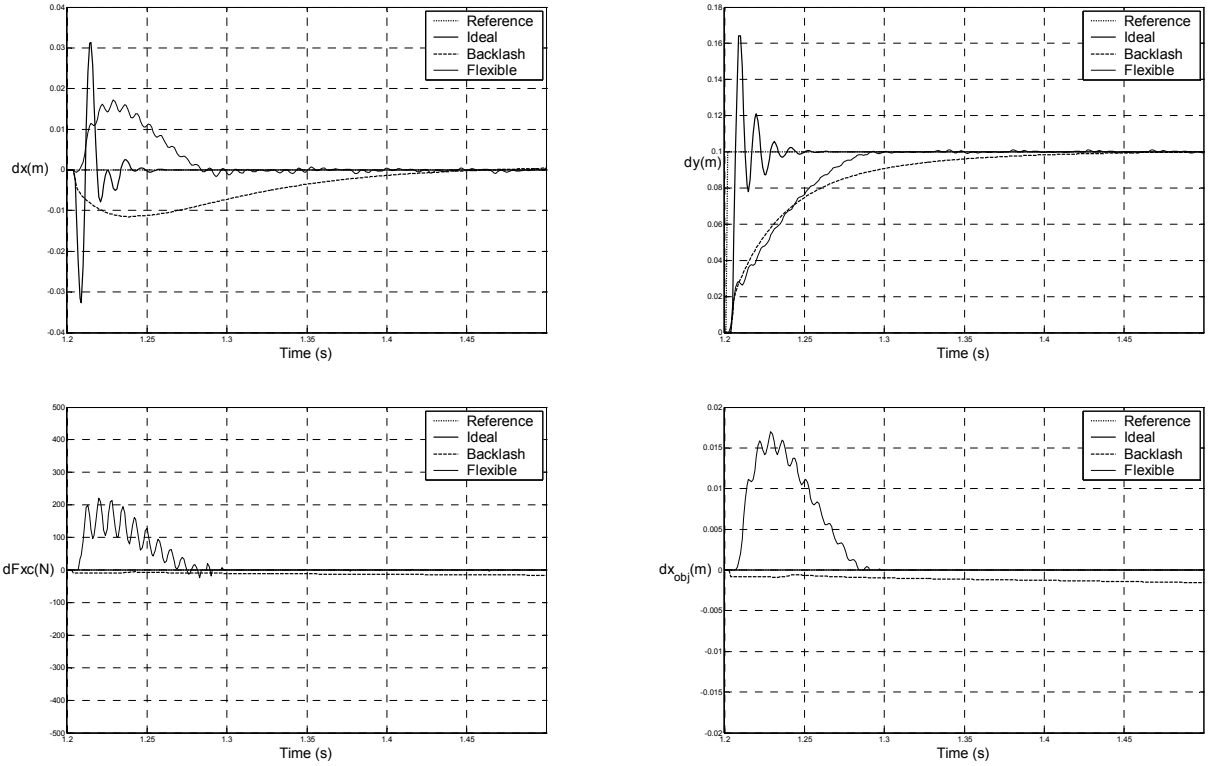

Figure 4 – Time response for the 2*R* ideal robot and robots with joints having backlash and flexibility under the action of the *PD – PI* algorithm for the *HC* and $\delta y_d = 10^{-3}$m.

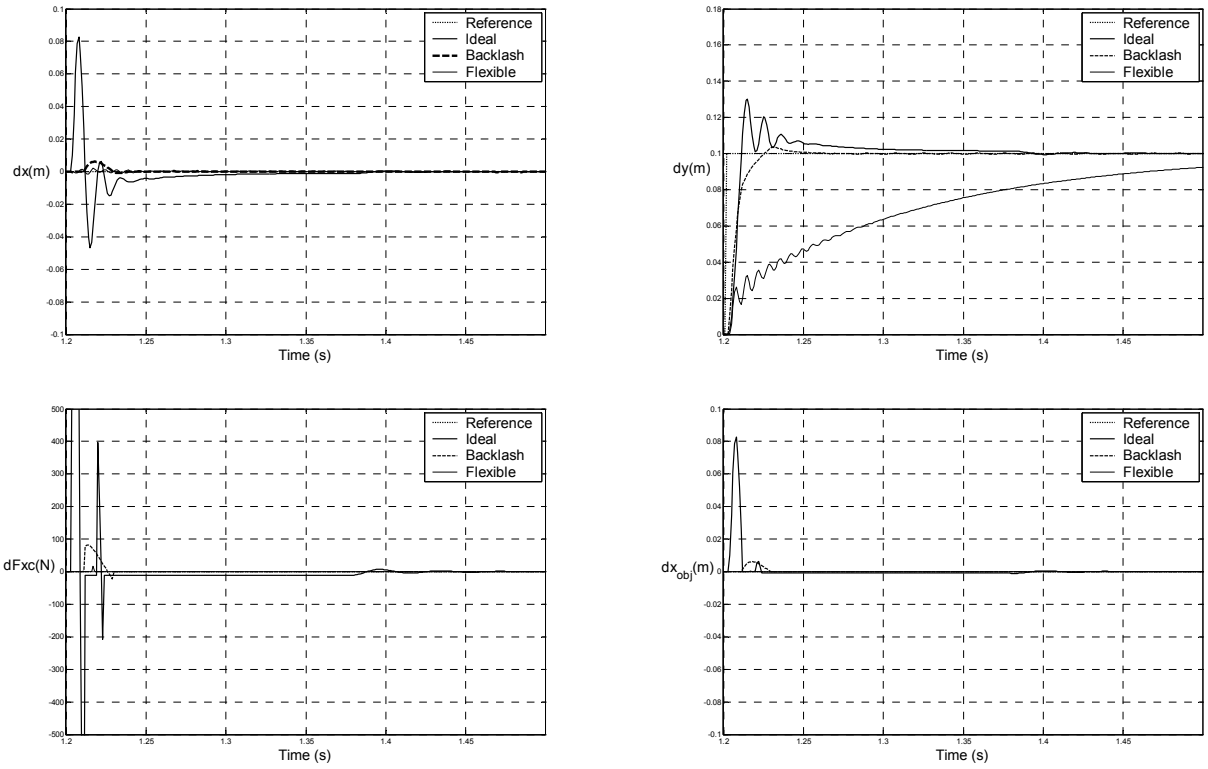

Figure 5 – Time response for the 2*R* ideal robot and robots with joints having backlash and flexibility under the action of the *FO* algorithm for the *HC* and $\delta y_d = 10^{-3}$m.

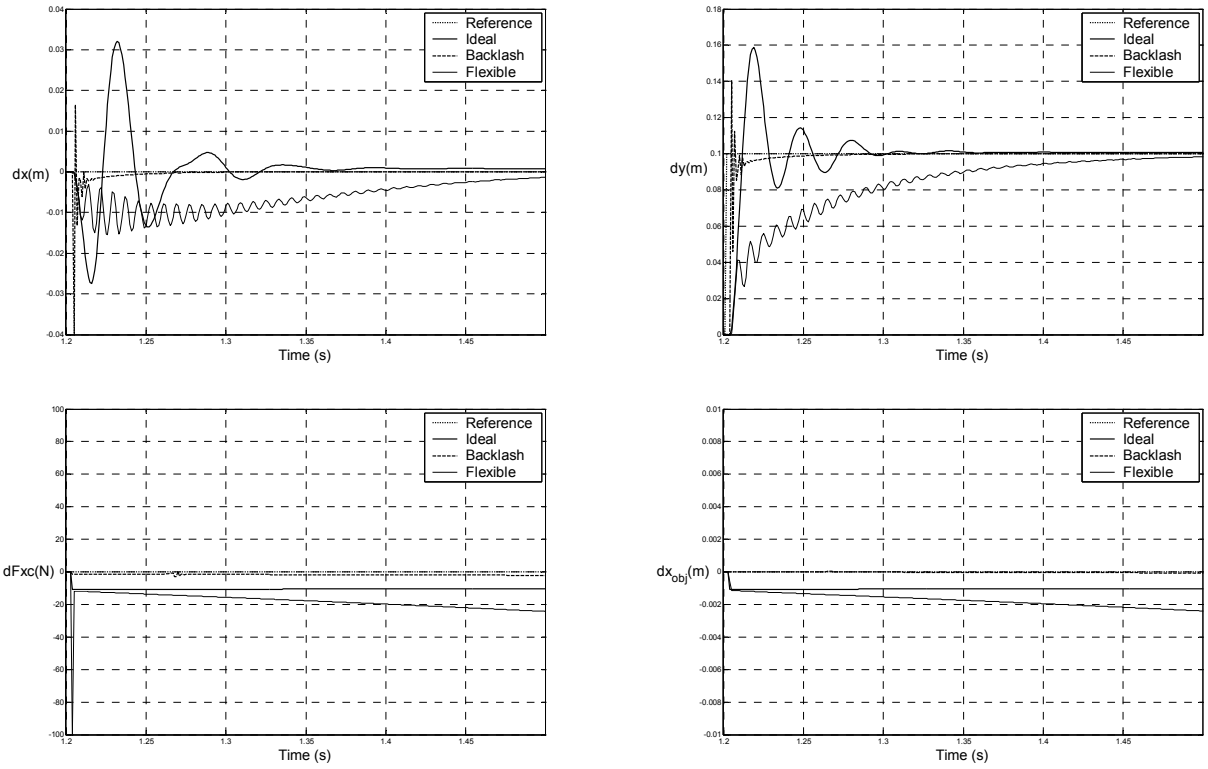

Figure 6 – Time response for the 2*R* ideal robot and robots with joints having backlash and flexibility under the action of the *PD*−*PI* algorithm for the *CC* and $\delta y_d = 10^{-3}$m.

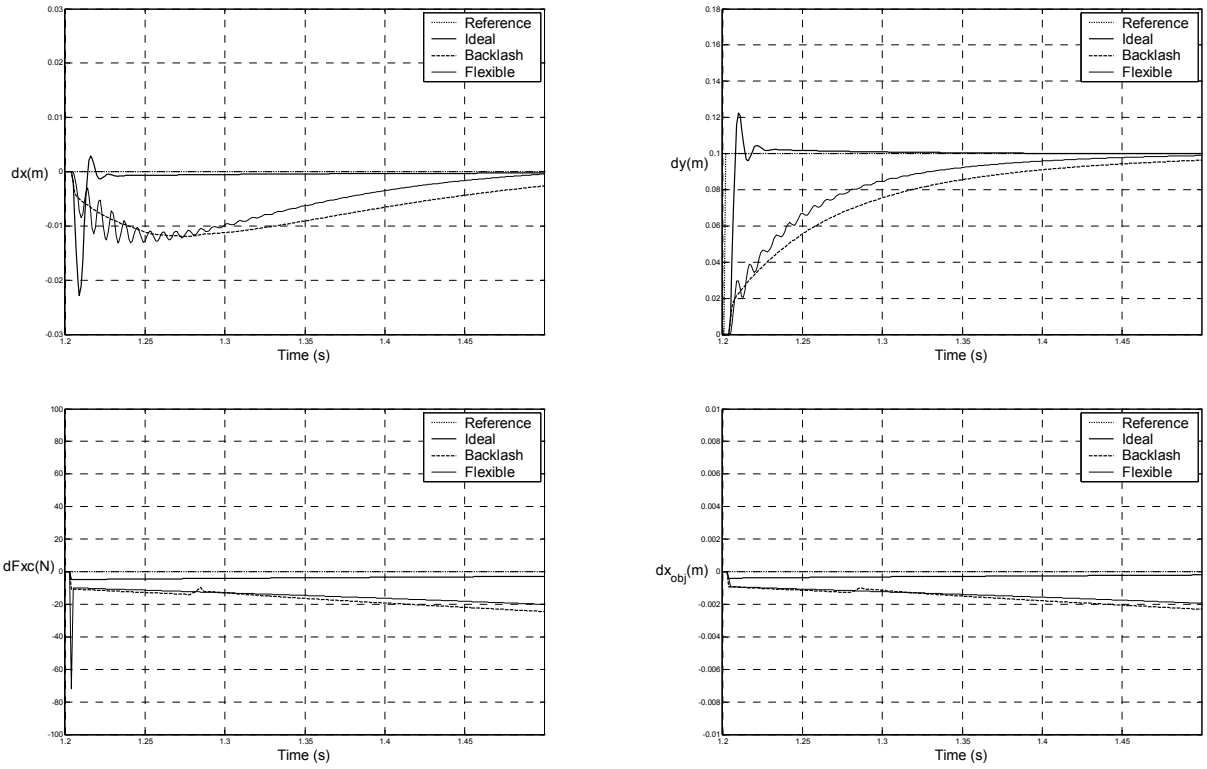

Figure 7 – Time response for the 2*R* ideal robot and robots with joints having backlash and flexibility under the action of the *FO* algorithm for the *CC* and $\delta y_d = 10^{-3}$m.

To compare the *HC* and the *CC* architectures, we repeat the experiment for the *FO* and *PD–PI* algorithms, and we analyses the variation of the position $\{x,y\}$ and force F of the robot and also the variation of the surface restriction xc_{obj}.

B. Frequency response

Figures 8 – 10 show the transfer functions $|Y_c(j\omega)/Y_{cd}(j\omega)|$, $|F_c(j\omega)/F_{cd}(j\omega)|$, $|Y_c(j\omega)/F_{cd}(j\omega)|$ and $|F_c(j\omega)/Y_{cd}(j\omega)|$ (where $Y_c(j\omega)=F\{\delta y_c\}$ and $F_c(j\omega)=F\{\delta F_c\}$) for the *FO* and the *PD*/*PI* controllers, in the cases of an ideal robot and a robot with flexibility at the joints, respectively.

The low-pass characteristics of $|Y_c(j\omega)/Y_{cd}(j\omega)|$ and $|F_c(j\omega)/F_{cd}(j\omega)|$ reveal the existence of some coupling between the position and force loops due to the non-ideal performance of both algorithms.

Figures 8 and 10 show the frequency responses for robots with ideal joints and transmissions having flexibility, both under the action of the *FO* and the *PD*/*PI* controllers, for a pulse perturbation, at the robot reference δy_d. We can see that the system with the *PD/PI* controllers has an higher overshoot and that the effect of the flexibility in high frequencies.

The charts reveal that the *FO* algorithms have a superior performance, namely a good robustness and larger bandwidth.

5. Summary and Conclusions

This paper presented the implementation of hybrid and cascade controllers for manipulators with several types of nonlinear phenomena at the joints. The system was tested both for fractional and integer order control algorithms.

The results show that the fractional order control algorithms have superior performances; the cascade algorithm method for force control is more stable than the hybrid position/force and scheme.

References

[1] M. H. Raibert and J. J. Craig, "Hybrid Position/Force Control of Manipulators", *ASME Journal of Dynamic Systems, Measurement, and Control*, vol. 102, no. 2, pp. 126–133, 1981.

[2] O. Khatib, "A Unified Approach for Motion and Force Control of Robot Manipulators: The Operational Space Formulation", *IEEE Journal of Robotics and Automation*, vol. 3, no. 1, pp. 43–53, 1987.

[3] B. Siciliano and L. Villani, "A Force/Position Regulator for Robot Manipulators without Velocity Measurements", *IEEE Int. Conf. on Robotics and Automation*, USA, 1996.

[4] H. Bruyninckx and J. De Schutter, "Specification of Force-Controlled actions in the Task Frame Formalism - A Synthesis", IEEE Trans.

on Robotics Automation, vol. 12, no. 4, pp. 581-589, 1996.

[5] M. M. Bridges, J. Cai, D. M. Dawson and M. T. Grabble, "Experimental Results for a Robust Position and Force Controller Implementation on a Direct Drive Robot", Robotica, vol. 13, no. 1, pp. 11-18, 1995.

[6] A. Oustaloup, *La Commande CRONE: Commande Robuste d'Ordre Non Entier*, Hermes, 1991.

[7] J. Tenreiro Machado, "Analysis and Design of Fractional-Order Digital Control Systems", *J. Systems Analysis, Modelling and Simulation*, vol. 27, pp. 107–122, 1997.

[8] N. Ferreira, J. Tenreiro Machado "Fractional-Order Hybrid Control of Robotic Manipulators*" The 11th International Conference on Advanced Robotics IEEE,* Coimbra, Portugal, pp. 393–398, 2003.

[9] I. Podlubny, "Fractional-Order Systems and $PI^{\lambda}D^{\mu}$-Controllers", *IEEE Transactions on Automatic Control*, vol. 44, no. 1, pp. 208–213, 1999.

[10] S. Dubowsky, J. F. Deck and H. Costello, "The Dynamic Modelling of Flexible Spatial Machine Systems with Clearance Connections", *ASME Journal of Mechanisms, Transmissions and Automation in Design,* vol. 109, no. 1, pp. 87–94, 1987.

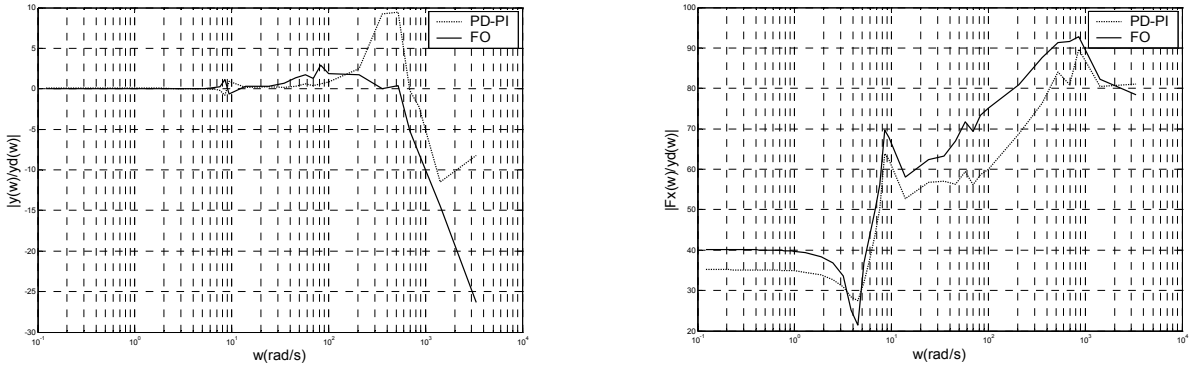

Figure 8 – Frequency responses for the ideal robot under the action of the *FO* and the *PD*/*PI* controllers for the *HC* and $\delta y_d = 10^{-3}$m.

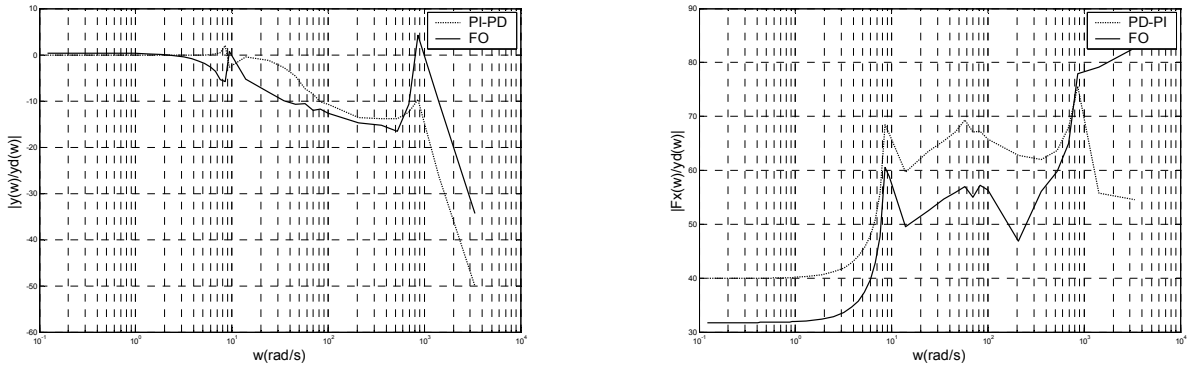

Figure 9 – Frequency responses for the robot with joints having flexibility, under the action of the *FO* algorithm, for the *HC* and $\delta y_d = 10^{-3}$m.

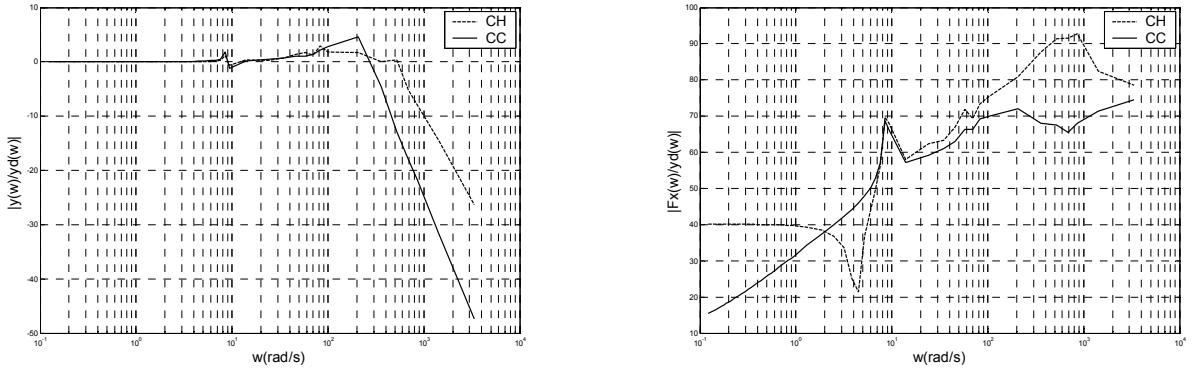

Figure 10 – Frequency responses for the ideal robot under the action of the *FO* algorithm, for the *HC* and *CC* architectures and $\delta y_d = 10^{-3}$m.